RSC Advances

PAPER

View Article Online
View Journal | View Issue

Cite this: *RSC Adv.*, 2017, **7**, 14060

Tribological properties of WS_2/graphene nanocomposites as lubricating oil additives

Dan Zheng,[a] Yan-ping Wu,[b] Zheng-yang Li[a] and Zhen-bing Cai*[a]

Received 12th December 2016
Accepted 16th February 2017

DOI: 10.1039/c6ra28028e

rsc.li/rsc-advances

In this study, we prepared a new composite material of graphene (GP) anchored with WS_2 nanoparticles (WS_2/GP). The lubricating potential of the as-prepared nanocomposites as oil additives was investigated with sliding steel-on-steel contact using a UMT-2 ball-on-plate tribotester. The oil dispersed with WS_2/GP displays remarkable lubricating performance; the friction coefficient and the wear rate were reduced by 70.2% and 65.8%, respectively, when 0.02–0.04 wt% WS_2/GP was added to the base oil. Its friction-reducing and anti-wear abilities were also superior to those of oil containing a single nanomaterial of GP or WS_2 nanoparticles (nano-WS_2) and oil dispersed with a physical mixture of nano-WS_2 and GP. WS_2/GP may deposit on the wear surfaces and form a protective film, which improves the contact state of the sliding interfaces. Moreover, a synergistic lubricating action between the GP and nano-WS_2 in the WS_2/GP nanocomposites was revealed. We suggest that these two nano-additives cooperatively work, which enhances the adsorption of GP layers and deposition of nano-WS_2, thereby resulting in an improved protective and repairing effect.

1 Introduction

The study of tribology, including friction, wear, and lubrication, has recently attracted significant attention because numerous mechanical system failures originate from wear and most non-renewable energy resource exhaustion results from friction.[1] The most effective approach to controlling or reducing friction and wear is to use a lubricant.[2] The preparation of lubricating materials with the simultaneous functions of friction reduction, anti-wear, and repair by combining micro/nanomaterials and lubrication is currently a hot research topic in lubrication science.

Graphene (GP), a 2D structure of single-atom-thick carbon,[3] has attracted significant attention because of its unique properties (including its superior strength,[4] good thermal conductivity,[5] good mechanical properties,[6] and remarkable electron-transporting properties[7–9]) in addition to its lubricating potential. The tribological properties of different types of GP nanosheets as effective solid lubricants were studied by Peng *et al.*[10] Klemenz *et al.*[11] performed nanoindentation and scratching of GP-covered Pt (111) surfaces in computer simulations and experiments and revealed the mechanisms of friction reduction and wear protection by GP on the atomic scale. Eswaraiah *et al.*[12] observed that the addition of ultrathin GP significantly improved the lubricating performance of engine oil. The frictional characteristics, anti-wear abilities, and extreme pressure properties of the GP-dispersed oil were improved by 80%, 33%, and 40%, respectively.

More recently, organically modified GP and GP–inorganic nanocomposites have been widely studied. Graphene oxide was modified with ionic liquids and ethylene glycol, and its tribological properties were evaluated by Kumar *et al.*[13,14] In addition, Su *et al.*[15,16] prepared Ni and Ag nanoparticle-decorated GP nanocomposites using a chemical reduction approach. Many studies have demonstrated that GP is a good supporter of nanoparticles, and as-prepared nanocomposites usually exhibit better lubricating performances than GP alone.

Previous studies have also shown that nanocomposites of GP and GP-like layered metal dichalcogenide nanoparticles exhibit remarkable physical and chemical properties, which is probably because of their structural compatibility and synergistic interactions.[17,18] However, research on the lubricating potential of these nanocomposites has rarely been reported. As a typical GP-like layered metal dichalcogenide, WS_2 has been widely studied because of its low cost, effectiveness in reducing friction and wear,[19–21] environmental compatibility, and excellent oxidation resistance.[22]

Motivated by the above considerations, we prepared WS_2 nanoparticle-decorated GP composites by adopting a facile and scalable approach and evaluated their lubricating performance on sliding steel-on-steel contacts using a UMT-2 ball-on-plate tribotester.

2 Experimental details

2.1 Materials

The GP used in this study was purchased from Jinan Graphene New Materials Co., Ltd. (Jinan, China) and was used as received. Commercial bulk WS_2 (purity ≥ 99.9%, particle size < 1 μm) was

[a]*Tribology Research Institute, Key Laboratory of Advanced Technologies of Materials (Ministry of Education), Southwest Jiaotong University, Chengdu 610031, China. E-mail: caizb@swjtu.cn*

[b]*China Academy of Engineering and Physics, Mianyang, 621900, China*

purchased from Huajing Powder Material Science & Technology Co., Ltd. (Changsha, China). NaCl, hydrochloric acid, ethanol, and deionized water were purchased from Chengdu Changzheng Glass Co., Ltd. (Chengdu, China) and were used as received.

PAO4 oil was used as a lubricant. The ball used for the tests was composed of GCr15 steel (wt%: 1.0C, 1.49Cr, 0.31Mn, 0.26Si, 0.009P, 0.004S) with a diameter of 9.525 mm and a hardness of 766 HV. The plate was composed of RTCr2 alloy cast iron (wt%: 3.11C, 2.21Si, 0.50Mn, 1.63Cr) with a hardness of 220 HV, which was cut into 25 × 12 × 6 mm sheets and subsequently polished to obtain a surface roughness of $R_a \leq 0.03$ μm.

2.2 Synthesis and characterization of WS_2/GP nanocomposites

To produce WS_2/GP nanocomposites, we first prepared WS_2 nanoparticles from bulk WS_2 using a mechanochemical treatment method.[23] In a typical procedure, 0.5 g WS_2 and 5.0 g NaCl were added to the agate grinding bowl of a planetary ball mill (JC-2, Nanan Jiacheng Electronic Technology Co., Ltd., Nanan, China) with a ball-to-feed ratio of 1 : 7. Ball milling was performed for 2 h at a rotation rate of 450 rpm at room temperature (RT). In this process, WS_2 was uniformly mixed with NaCl and became nanostructured after ball milling. The samples were then repeatedly washed with deionized water and ethanol before being dried under vacuum at 80 °C for 8 h to obtain the exfoliated WS_2 (exf-WS_2) nanoparticles.

In the subsequent step, the GP and exf-WS_2 were dispersed in deionized water with a mass ratio of 1 : 9; the mixture was then sonicated and stirred at RT for 1 h each using a KQ-700E ultrasonic system (Kunshan Ultrasonic Instruments Co., Ltd., Kunshan, China) and a REX magnetic stirrer (REX, Shanghai, China). To generate active functional sites, we dropped two drops of concentrated hydrochloric acid into the reaction mixture. We then stirred the mixture and sealed it in a 50 ml autoclave, which was maintained at 240 °C for 24 h. Finally, the resulting product, WS_2/GP, was filtered using a TG-16 high-speed centrifuge (Gongyi Yuhua Instrument Co., Ltd., Gongyi, China) and repeatedly washed with deionized water and ethanol before being freeze-dried for further use.

Scanning electron microscopy (SEM, JSM-7001F, JEOL, Japan) and transmission electron microscopy (TEM, JEM-2100F, JEOL, Japan) were used to characterize the morphologies and microstructures. X-ray diffraction (XRD) measurements were performed using an X'Pert Pro X-ray diffractometer (PANalytical, Holland) with an X-ray source of Ni-filtered Cu Kα radiation (1.54 Å) in the 2θ range 10–80° with a step size of 0.016. Raman spectra were recorded in the range 4000–400 cm^{-1} using a 532 nm laser as the excitation source on a Raman microscope system (LabRam HR, Renishaw, UK).

2.3 Tribological evaluation of WS_2/GP nanocomposites

In this study, GP, exf-WS_2 nanoparticles (nano-WS_2), and WS_2/GP nanocomposites (WS_2/GP) were dispersed into PAO4 oil as a lubricant under ultrasonication for 1 h. Inorganic nanoparticle additives are infamous for having poor dispersion stability in organic liquids, so the same concentration of surfactant Span-80 ($C_{24}H_{44}O_6$, Chengdu Changzheng Glass Co., Ltd.) was used as a dispersing agent. Fig. 1 presents digital pictures of different nano-additive dispersions with and without addition of Span-80 immediately after sonication and after 7 days undisturbed at 100 °C after sonication. A 0.1 wt% solution was selected for better observation. The dispersion test results show that Span-80 effectively allows these nano-additives to disperse well in PAO4 oil, and the best dispersion is exhibited by WS_2/GP with the second best being GP. PAO4 base oil was also used to provide a baseline for comparison. Tribological tests were performed with an applied load of 10 N, a sliding distance of 8 mm, and a speed of 5 mm s^{-1}. To accurately evaluate the tribological properties of the WS_2/GP nanocomposites as oil additives, all the tests were run for a relatively long time (6000 s) at a constant relatively high temperature (100 °C) in air. The parameters were selected to ensure boundary lubrication and to simulate high-load contact situations in components such as gears and bearings.[24] The upper ball and lower plate were fixed in a square tank equipped with the lubricating oil. The bottom of the tank was fitted with a heating device that could control the experimental temperature. Before each test, the balls and plates were cleaned with ethanol to keep the surfaces as clean as possible.

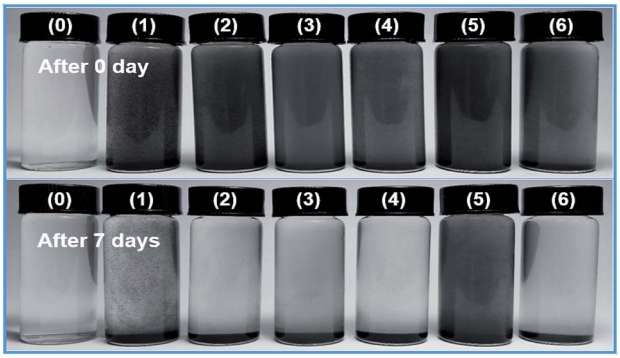

Fig. 1 Images of different nano-additive dispersions with and without addition of Span-80 immediately after sonication and after 7 days undisturbed at 100 °C after sonication: (0) pure PAO4, (1) PAO4 + 0.1 wt% GP + 0.1 wt% SP, (2) PAO4 + 0.1 wt% GP, (3) PAO4 + 0.1 wt% nano-WS_2 + 0.1 wt% SP, (4) PAO4 + 0.1 wt% nano-WS_2, (5) PAO4 + 0.1 wt% WS_2/GP + 0.1 wt% SP, and (6) PAO4 + 0.1 wt% WS_2/GP.

After the tests, the worn surfaces were cleansed and then analyzed using a 3D surface profilometer (NanoMap-D, AEP, USA) and optical microscope (OM, Olympus BX60M, Olympus, Japan). SEM, Raman, energy-dispersive X-ray spectroscopy (EDX, EDAX-7760/68M, JEOL, Japan), and X-ray photoelectron spectroscopy (XPS, ESCALAB 250Xi, Thermo Nicolet, USA) measurements were also used to characterize the worn surfaces.

3 Results and discussion

3.1 Morphology and microstructure

SEM images of GP, nano-WS_2, and WS_2/GP nanocomposites are presented in Fig. 2. The SEM image of GP reveals a wrinkled and

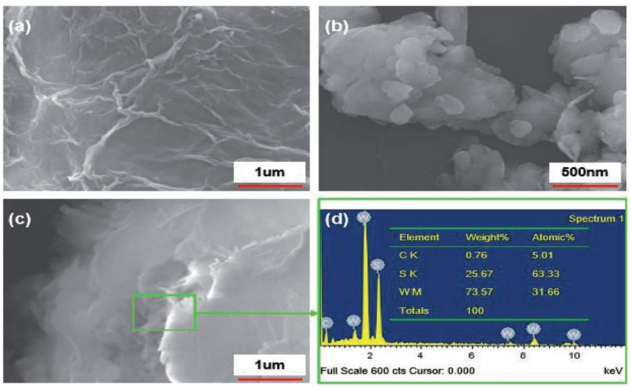

Fig. 2 SEM images of (a) GP, (b) nano-WS_2, and (c) WS_2/GP; (d) EDX analysis of WS_2/GP.

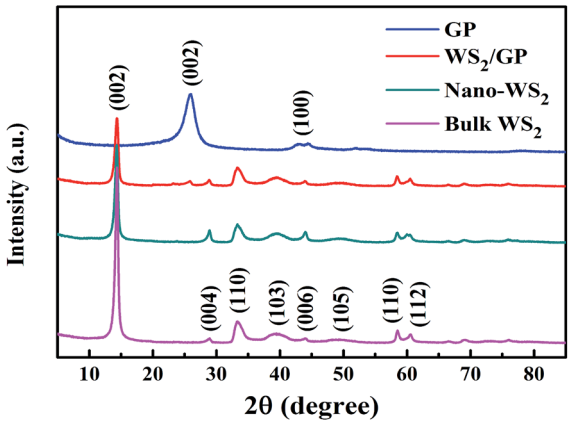

Fig. 4 XRD patterns of bulk WS_2, GP, nano-WS_2, and WS_2/GP.

layered morphology (Fig. 2a), whereas nanoscale patchy particles are observed in the nano-WS_2 image (Fig. 2b). The image of WS_2/GP in Fig. 2c reveals overlapping and interweaving of sheets of GP and nano-WS_2, which is further confirmed by the EDX results in Fig. 2d.

Fig. 3 presents TEM and HRTEM images of GP, nano-WS_2, and WS_2/GP. The GP image reveals a few-layered and wrinkled structure (Fig. 3a), with an interlayer distance of 0.34 nm, corresponding to the (002) plane (Fig. 3b). A nanoscale patchy structure of nano-WS_2 with a size distribution of below 100 nm is visible in Fig. 3c. Fig. 3d indicates that the interlayer distance is 0.62 nm, corresponding to the (002) plane. In Fig. 3e, loading of nano-WS_2 on the surfaces of GP is observed, resulting in a layer-by-layer hybrid structure of WS_2/GP. Moreover, two different interlayer distances of 0.34 and 0.62 nm are simultaneously observed, as labeled in Fig. 3f.

To examine the fine microstructure, bulk WS_2, GP, nano-WS_2, and WS_2/GP samples were characterized using XRD and Raman analyses. Fig. 4 presents the XRD patterns of the samples. All the peaks of bulk WS_2 can be attributed to the hexagonal phase (JCPDS no. 08-0237), indicating its high purity. Strong (002) diffraction peaks of the bulk WS_2, nano-WS_2, and WS_2/GP are observed at 14.4°, indicating their well-stacked layered structure. However, both the nano-WS_2 and WS_2/GP display much less intense (002) peaks than the bulk WS_2, indicating that their crystallite size and the number of layers are much smaller.[25] For GP, the C (002) characteristic peak of GP appears at 25.9°. Furthermore, all the peaks of nano-WS_2 are detected in the WS_2/GP XRD pattern, and a new peak at 25.9°, corresponding to the C (002) peak, is also observed.

Fig. 5a presents the Raman spectra of the GP, nano-WS_2, and WS_2/GP. Two dominant peaks of nano-WS_2 are observed at 353 and 419 cm^{-1}, corresponding to the E1 2g and A_{1g} modes of the hexagonal WS_2, respectively.[26] For GP, the GP characteristic D, G, and 2D peaks are observed. The appearance of the D peak proves that a significant number of defects exist.[27] In the spectrum of WS_2/GP, the E1 2g and A_{1g} peaks as well as the D and G peaks can be detected. Additionally, the D peak of GP corresponds to sp^3/sp^2 hybridized defects, whereas the G peak

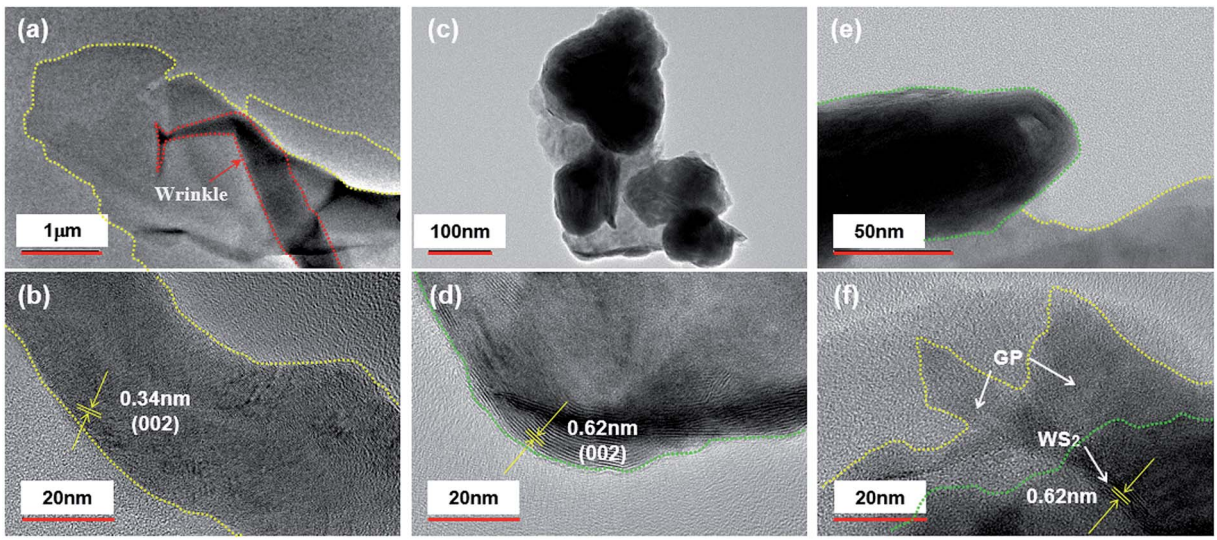

Fig. 3 TEM and HRTEM images of (a and b) GP, (c and d) nano-WS_2, and (e and f) WS_2/GP.

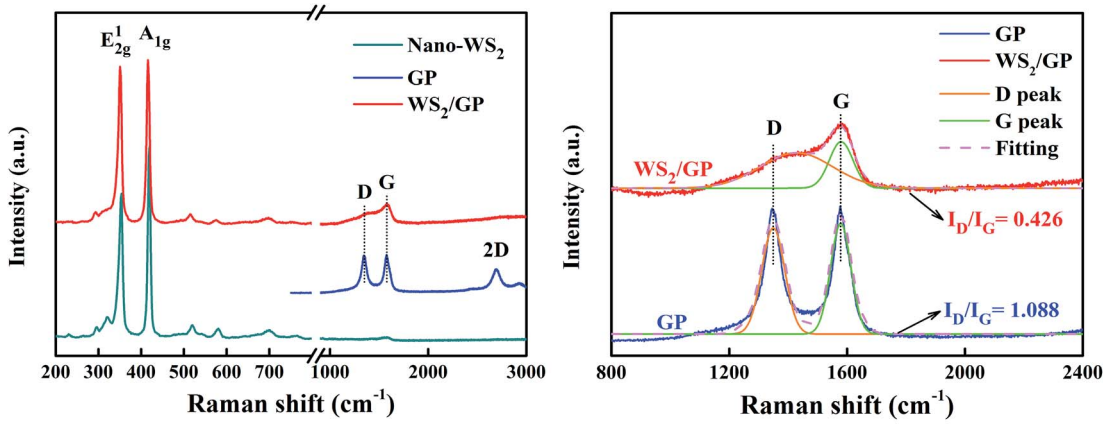

Fig. 5 (a) Raman spectra of GP, nano-WS_2, and WS_2/GP and (b) magnification and Gaussian fitting of the D and G peaks of the Raman spectra of GP and WS_2/GP.

corresponds to vibration in all of the sp^2-bonded carbon atoms.[28] Thus, magnification and Gaussian fitting of the D and G peaks of GP and WS_2/GP as well as the intensity ratio of the D peak to the G peak (I_D/I_G) are compared in Fig. 5b. The I_D/I_G of WS_2/GP was significantly reduced (from 1.088 to 0.426), revealing that the GP defects were repaired by nano-WS_2.

In summary, these findings confirm the successful preparation of WS_2/GP nanocomposites; it is reasonable to conclude that the GP and nano-WS_2 are chemically linked by π–π interactions.

3.2 Friction and wear

We first investigated the lubricating abilities of GP and nano-WS_2 separately. Fig. 6 shows a plot of the average friction coefficients when lubricated with different concentrations of GP-dispersed oil and nano-WS_2-dispersed oil. The friction coefficient (COF) was effectively reduced after adding GP or nano-WS_2, and the COF reduction reached a maximum at the same concentration of 0.01 wt%, which was considered to be the optimal concentration of these two additives and was thus selected for investigation of the lubricating potential of WS_2/GP nanocomposites. However, further increase in the concentration increased the COF, especially for nano-WS_2, which was probably because the inhomogeneity of the lubricant resulted from unstable dispersion.[29]

The friction coefficient curves of the PAO4 base oil and oils dispersed with 0.01 wt% GP, nano-WS_2, and WS_2/GP are presented in Fig. 7a. A physical mixture of GP and nano-WS_2 with a mass-ratio of 1 : 9 (WS_2 + GP) was also used at the same concentration for comparison. All the dispersed oils exhibited smaller and more stable friction coefficients than the base oil. However, the additives resulted in different friction-reducing efficiencies. The WS_2/GP-dispersed oil exhibited the lowest friction coefficient, followed by the WS_2 + GP-dispersed oil.

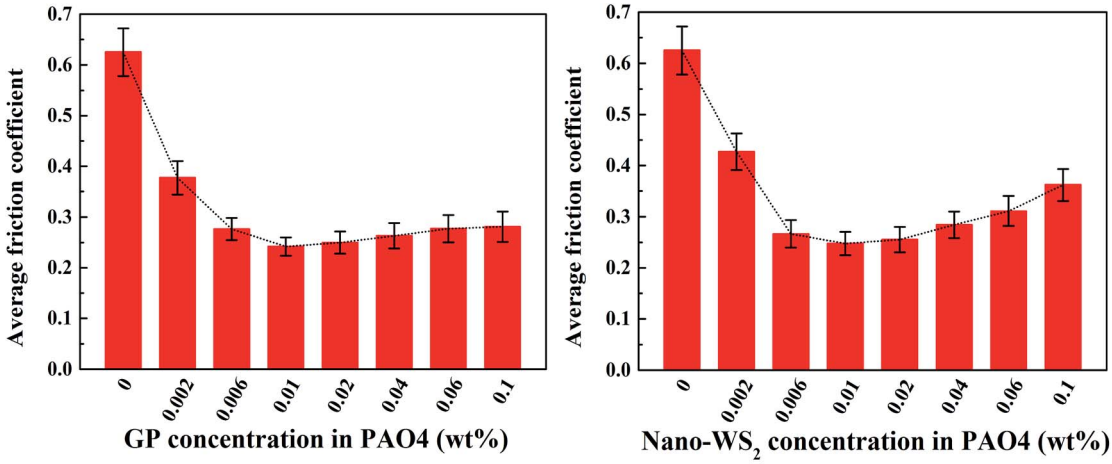

Fig. 6 Average friction coefficient using different concentrations of (a) GP-dispersed oil and (b) nano-WS_2-dispersed oil lubrication.

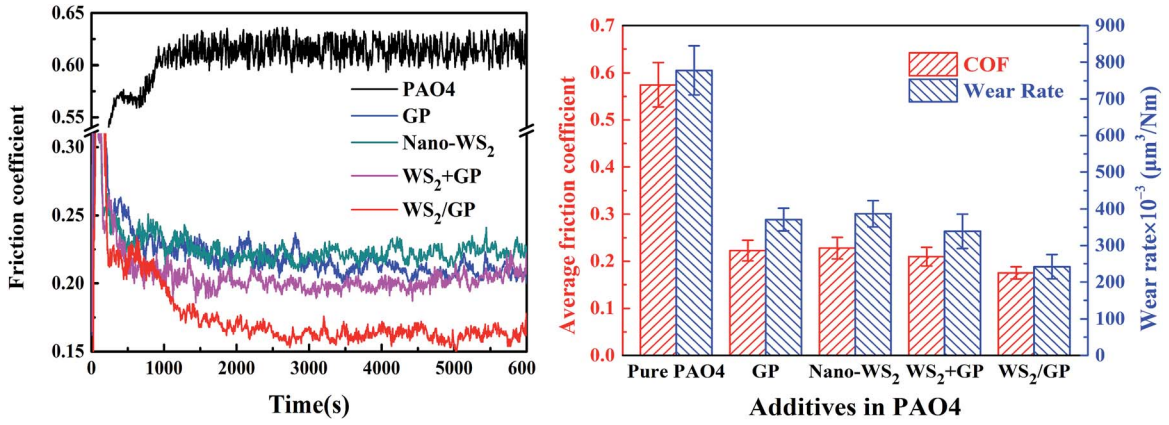

(a) (b)

Fig. 7 (a) Friction coefficient curves for PAO4 base oil and dispersed oils containing 0.01 wt% GP, nano-WS_2, WS_2 + GP, and WS_2/GP. (b) Comparisons of the average friction coefficients and corresponding wear rates after lubrication with these oils.

Comparisons of the average friction coefficients and wear rates using these oils are shown in Fig. 7b. All the nano-additives improve the lubricating performance of the base oil. However, the oil dispersed with WS_2/GP exhibits the most outstanding potential; its friction coefficient and wear rate were reduced by 70.2% and 65.8%, respectively, compared with the base oil. Fig. 7b also suggests that WS_2/GP has a better lubricating performance than GP or nano-WS_2 alone. This finding may originate from the synergistic lubricating action of the two components. Additionally, a certain degree of friction and wear reduction was also caused by WS_2 + GP compared with GP or nano-WS_2 alone; however, this was far less significant than that of WS_2/GP. This finding also confirms that WS_2/GP is a new composite material rather than a simple physical mixture.

Fig. 8a shows the friction coefficient curves of the WS_2/GP dispersed oils with different concentrations. The average friction coefficients and corresponding wear rates are compared in Fig. 8b. Similar "deep valley" shapes were observed for the variations; the lowest friction coefficient and wear rate appear at 0.02 wt% and 0.04 wt%, respectively. The optimal concentration of WS_2/GP is considered to be in the range 0.02–0.04 wt%. It cannot be overlooked that this optimal concentration is considerably higher than that of GP or nano-WS_2, which is probably because of the better dispersion of WS_2/GP. In summary, an excellent lubricating performance can be achieved with WS_2/GP-dispersed oil, which is maximized at concentrations of 0.02–0.04 wt%.

3.3 Worn surface characterization

After the tests, the worn surfaces of the plates using the PAO4 base oil and dispersed oils containing 0.01 wt% GP, nano-WS_2, WS_2 + GP, and WS_2/GP were analyzed using SEM, and the results are shown in Fig. 9. In Fig. 9a and b, the wear scar of the plate lubricated with the base oil is the largest; the worn surface is very rough and displays deep machining marks and severe

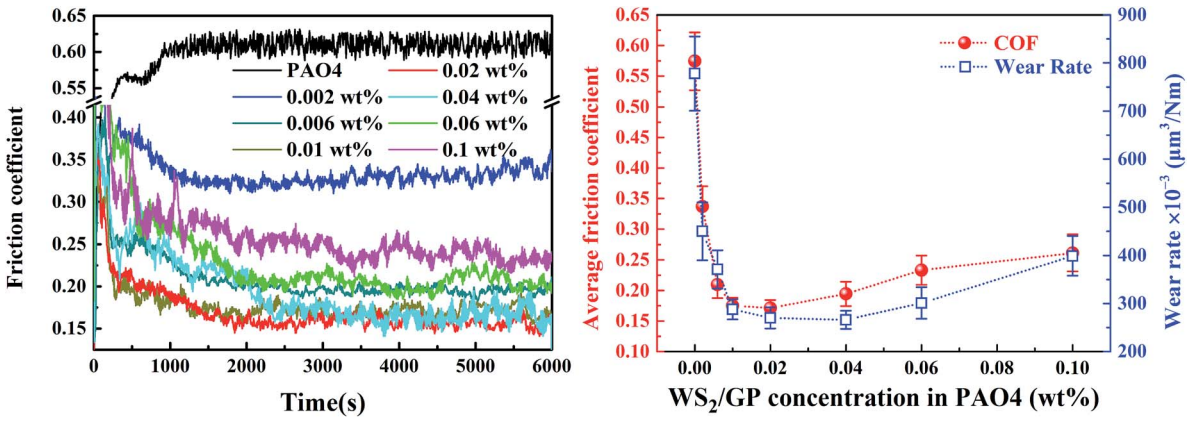

(a) (b)

Fig. 8 (a) Friction coefficient curves and (b) variations of the average friction coefficients and corresponding wear rates after lubrication with different concentrations of the WS_2/GP-dispersed oil.

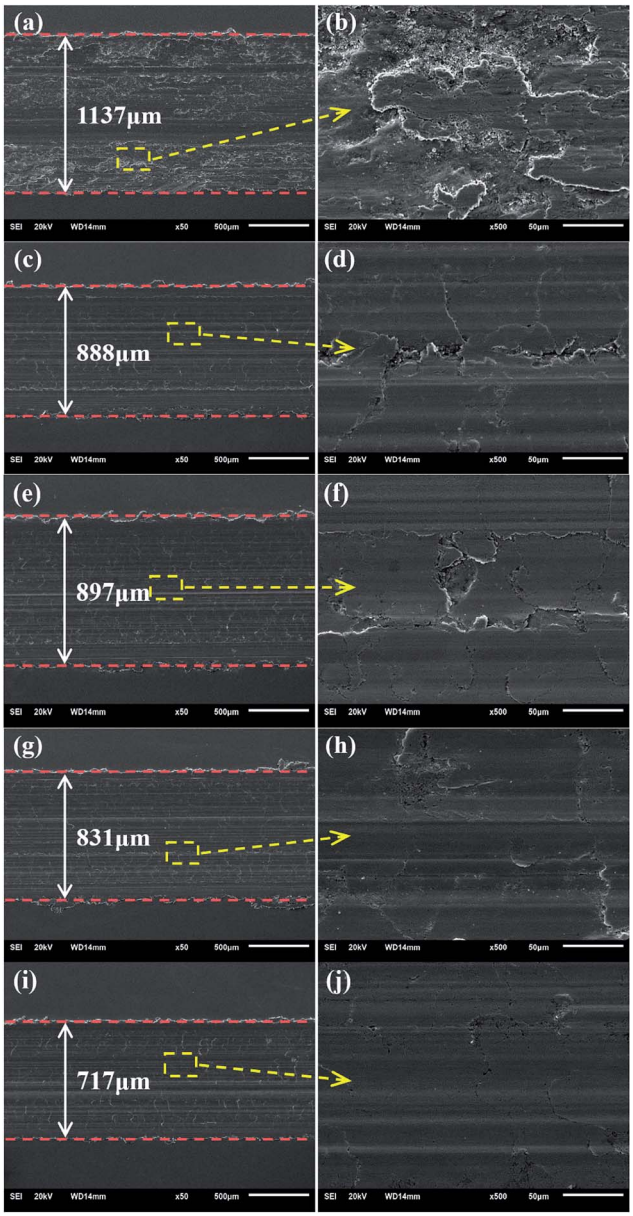

Fig. 9 SEM images at different magnifications of the worn surfaces of the plates lubricated with different oils: (a and b) PAO4 base oil, (c and d) 0.01 wt% GP-dispersed oil, (e and f) 0.01 wt% nano-WS_2-dispersed oil, (g and h) 0.01 wt% WS_2 + GP-dispersed oil and (i and j) 0.01 wt% WS_2/GP-dispersed oil.

material spallation. After adding GP, the width of the wear scar was reduced, the defects became relatively shallower and narrower, and the worn surface became smoother despite the presence of machining marks (Fig. 9c and d). The worn plate lubricated with the nano-WS_2-dispersed oil displays slightly rough surfaces with certain machining marks (Fig. 9e and f). GP and nano-WS_2 are considered to have similar lubricating ability. As observed in Fig. 9g and i, the plates lubricated with the WS_2 + GP- and WS_2/GP-dispersed oil display much smaller wear scar widths than those using GP or nano-WS_2 alone; their worn surfaces are significantly smoother, and the defects are not obvious (Fig. 9h and j). However, it is apparent that WS_2/GP had

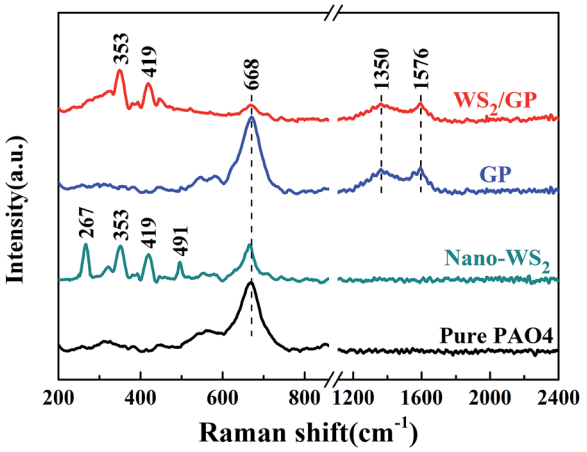

Fig. 10 Raman spectra of the wear scars of plates lubricated with PAO4 base oil and dispersed oils containing 0.01 wt% GP, nano-WS_2, and WS_2/GP.

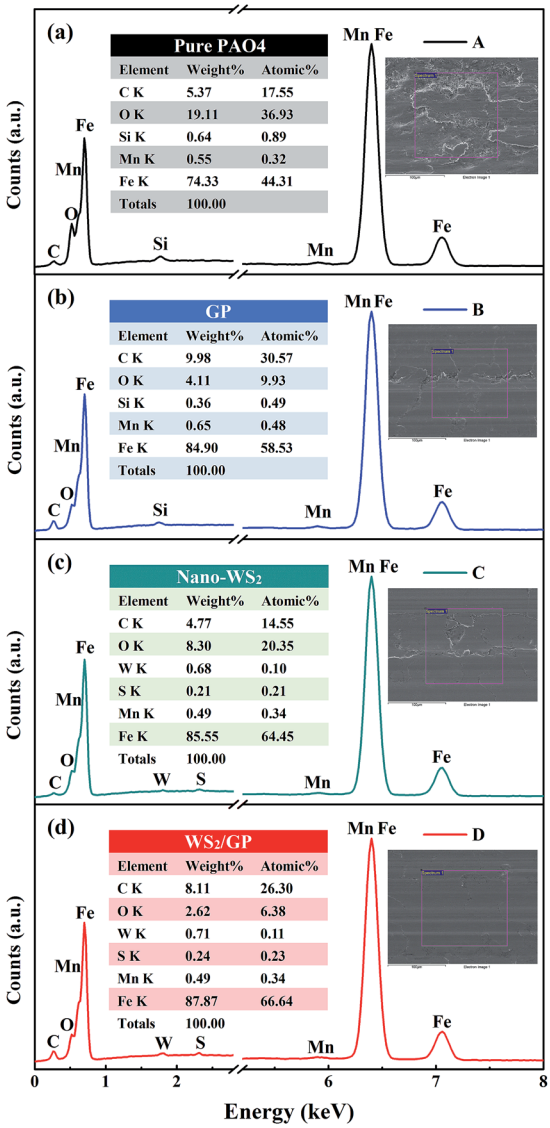

Fig. 11 EDX spectra of the wear scars of plates lubricated with (a) PAO4 base oil, (b) 0.01 wt% GP-dispersed oil, (c) 0.01 wt% nano-WS_2-dispersed oil, and (d) 0.01 wt% WS_2/GP-dispersed oil.

better lubricating ability than WS_2 + GP; the worn surface lubricated with the WS_2/GP-dispersed oil is very smooth without obvious defects.

Fig. 10 presents Raman spectra of the wear scars of the plates lubricated with the PAO4 base oil and the dispersed oils containing 0.01 wt% GP, nano-WS_2, and WS_2/GP. For the wear scar of the plate lubricated with the base oil, a typical peak of iron oxide was detected at 668 cm^{-1}. Considering that severe wear occurred, adhesive wear was the dominant mechanism of wear. After adding GP, it can be concluded that the GP layers adsorbed on the sliding interfaces during the frictional process as evidenced by the appearance of D and G peaks. A protective film may have been formed, which explains the friction and wear reduction. In addition, the typical peak of iron oxide was also observed, indicating that severe oxidation occurred. For the wear scar of the plate lubricated with the nano-WS_2-dispersed oil, typical peaks at 353 and 419 cm^{-1}, which were attributed to the E1 2g and A_{1g} modes of nano-WS_2, were observed. However, two new peaks at 267 and 491 cm^{-1} emerged after friction, which were attributed to the reaction products of nano-WS_2,[30] indicating that nano-WS_2 reacted with the substrate or molecules of the base oil. Remarkably, the typical peak of iron oxide was obviously weakened. This finding indicates that the deposition, self-repair, and formation of the chemical reaction film may be the main causes of the friction-reduction and anti-wear properties of nano-WS_2. When the surface was lubricated with the WS_2/GP-dispersed oil, the characteristic peaks of nano-WS_2 at 353 and 419 cm^{-1} and the characteristic peaks of GP at 1350 and 1576 cm^{-1} could be simultaneously detected. Additionally, no clear peaks of the reaction products of nano-WS_2 were observed, suggesting that GP helps to protect nano-WS_2 from tribochemical reactions. Furthermore, the typical peak of iron oxide was undetectable. Remarkably, the intensity reduction of the characteristic peaks of GP was not obvious compared with that of the GP-dispersed oil, which is unexpected even though the concentration of GP was one order of magnitude lower.

Fig. 11 shows the elemental distribution in the wear scars of the plates lubricated with these oils, as detected by SEM-EDX. The lowest Fe content was observed for the wear scar generated with the base oil and a strong peak for O was detected, which indicated that severe tribo-oxidation of the substrate occurred. After adding GP, a strong peak for C was observed, indicating that the GP layers adsorbed on the sliding interfaces. After adding nano-WS_2, peaks of W and S as well as relatively high O and Fe contents were observed. Most likely, a deposited film and a chemical reaction film of nano-WS_2 were formed on the sliding interfaces. When the plate was lubricated with the WS_2/GP-dispersed oil, peaks of W and S were also detected. In addition, the lowest O and highest Fe contents were observed, and a strong C peak was detected. These findings further demonstrate the synergistic effect of these two nano-additives on reducing the friction and wear.

XPS analysis was performed to explore the lubricating mechanism of this composite additive. Fig. 12 presents the full spectrum and curve-fitted XPS spectra of C1s, O1s, Fe2p, W3d, and S2p on the wear scar of the plate lubricated with 0.01 wt% WS_2/GP-dispersed oil. In Fig. 12b, the two C1s peaks, which matched well with the sp^3-C (C–C/O) and sp^2-C (C=C/O)[31]

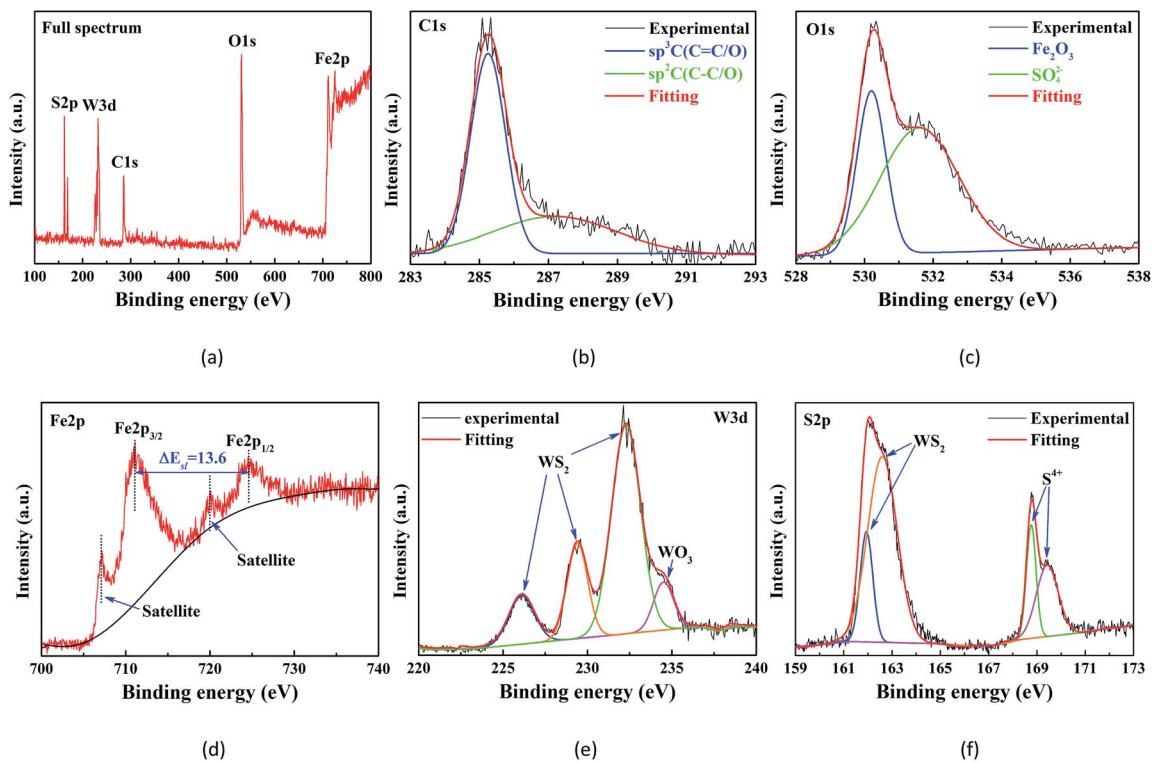

Fig. 12 (a) XPS full spectrum and curve-fitted XPS spectra of (b) C1s, (c) O1s, (d) Fe2p, (e) W3d, and (f) S2p of the wear scar of the plate lubricated with 0.01 wt% WS_2/GP-dispersed oil.

signals, may originate from the WS_2/GP nanocomposites. Therefore, we can reasonably conclude that the GP of the nanocomposites was deposited on the contact surfaces and formed a physical protective film. The O1s peak at 532.1 eV in Fig. 12c was indexed to sulfates, suggesting that a chemical transfer film may have been formed on the worn surfaces.

This conjecture is further authenticated by the WO_3 signal in the W3d peak (Fig. 12e) and S^{4+} signal in the S2p peak (Fig. 12f). In addition, the other O1s peak at 530.4 eV was attributed to Fe_2O_3. The $Fe2p_{3/2}$ and $Fe2p_{1/2}$ signals positioned at 711.1 and 724.7 eV, respectively, belonged to the Fe2p of the Fe_2O_3 groups. These findings confirm that the tribo-oxidation of the substrate cannot be prevented completely. Furthermore, the WS_2 signals in the W3d peak and S2p peak can only originate from the WS_2/GP nanocomposites, which might be due to the deposition of nano-WS_2 of the WS_2/GP nanocomposites.

3.4 Synergistic lubricating mechanism

In order to intuitively compare the lubricating abilities of the nano-additives, a simplified polar coordinate method was used, based on the above characterization and analysis results, as shown in Fig. 13. Three lubricating mechanisms, self-repairing, adsorption, and tribochemistry, as well as the dispersibility were used as evaluation indexes and were roughly divided into three grades: I, II, and III, where I is inferior and III is superior. In the GP-dispersed oil, the GP layers sheared at the sliding interfaces and adsorbed, which is attributed to its 2D structure;[32–34] a protective film may be formed, which results in low friction and wear. In the nano-WS_2-dispersed oil, the main lubricating mechanism was a frictional chemical reaction and deposition and self-repair of the nano-WS_2. When lubricated with the WS_2/GP-dispersed oil, a combined effect of GP and nano-WS_2 in the WS_2/GP nanocomposites was observed during the frictional process. This phenomenon resulted in enhanced adsorption of GP layers and deposition of nano-WS_2, which played a role in the protection and restoration and yielded a synergistic lubricating mechanism.

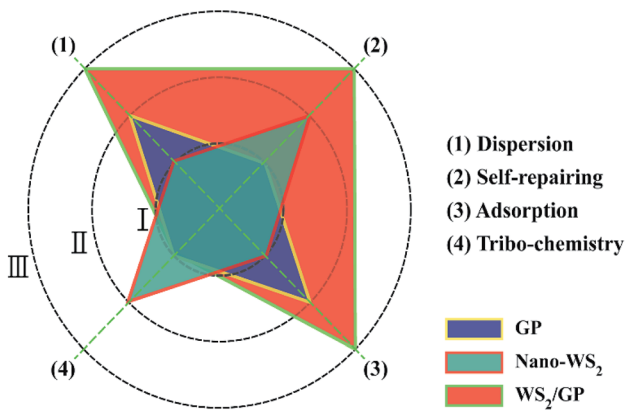

Fig. 13 Comparison of the lubricating mechanisms of the GP, nano-WS_2, and WS_2/GP nano-additives using a simplified polar coordinate method.

4 Conclusions

In summary, composites of GP anchored with WS_2 nanoparticles were successfully prepared, and these displayed better dispersion in the base oil than GP or nano-WS_2 alone. The addition of WS_2/GP significantly improves the lubricating performance of the base oil. The friction coefficient and wear rate were reduced by 70.2% and 65.8%, respectively, when 0.02–0.04 wt% WS_2/GP was dispersed. The friction-reducing and anti-wear abilities of WS_2/GP were also superior to those of GP or nano-WS_2 alone as well as to a physical mixture of the two additives. During the frictional process, the WS_2/GP is deposited on the wear surfaces and forms a protective film that improves the contact state of the sliding interfaces. Moreover, the GP and nano-WS_2 in the WS_2/GP nanocomposites work cooperatively to create a synergistic lubricating action, resulting in better protective and repairing effects. Thus, the adsorption of GP layers and deposition of nano-WS_2 were both enhanced, which is the crucial factor leading to the super-lubricating performance of WS_2/GP nanocomposites. The above results not only suggest the use of WS_2/GP nanocomposites as potential additives to improve the lubricating performance of oil-based lubricants but also provide new ideas for research on the lubricating potential of nanocomposites of GP and GP-like nanoparticles.

Acknowledgements

This study was supported by the National Science Foundation of China (51375407 and U1530136).

References

1 S. Zhang, *China Surf. Eng.*, 2008, **21**(2), 50–52.
2 D. Berman, A. Erdemir and A. V. Sumant, *Mater. Today*, 2014, **17**(1), 31–42.
3 K. S. Novoselov, A. K. Geim, S. V. Morozov, D. Jiang, Y. Zhang, S. V. Dubonos and A. A. Firsov, *Science*, 2004, **306**(5696), 666–669.
4 C. Lee, X. Wei, J. W. Kysar and J. Hone, *Science*, 2008, **321**(5887), 385–388.
5 H. Liem and H. S. Choy, *Solid State Commun.*, 2013, **163**(6), 41–45.
6 M. Naebe, J. Wang, A. Amini, H. Khayyam, N. Hameed, L. H. Li and B. Fox, *Sci. Rep.*, 2014, **4**, 4375.
7 F. Withers, T. H. Bointon, M. Dubois, S. Russo and M. F. Craciun, *Nano Lett.*, 2011, **11**(9), 3912–3916.
8 H. Park, P. R. Brown, V. Bulović and J. Kong, *Nano Lett.*, 2011, **12**(1), 133–140.
9 D. Ponnamma, Q. Guo, I. Krupa, M. A. S. A. Al-Maadeed, K. T. Varughese, S. Thomas and K. K. Sadasivuni, *Phys. Chem. Chem. Phys.*, 2015, **17**(6), 3954–3981.
10 Y. Peng, Z. Wang and K. Zou, *Langmuir*, 2015, **31**(28), 7782–7791.
11 A. Klemenz, L. Pastewka, S. G. Balakrishna, A. Caron, R. Bennewitz and M. Moseler, *Nano Lett.*, 2014, **14**(12), 7145–7152.

12 V. Eswaraiah, V. Sankaranarayanan and S. Ramaprabhu, *ACS Appl. Mater. Interfaces*, 2011, **3**(11), 4221–4227.
13 R. Gusain, H. P. Mungse, N. Kumar, T. R. Ravindran, R. Pandian, H. Sugimura and O. P. Khatri, *J. Mater. Chem. A*, 2016, **4**(3), 926–937.
14 B. Gupta, N. Kumar, K. Panda, A. A. Melvin, S. Joshi, S. Dash and A. K. Tyagi, *J. Phys. Chem. C*, 2016, **120**(4), 2139–2148.
15 Y. Meng, F. Su and Y. Chen, *ACS Appl. Mater. Interfaces*, 2015, **7**(21), 11604–11612.
16 Y. Meng, F. Su and Y. Chen, *Sci. Rep.*, 2016, **6**, 31246.
17 D. Chen, W. Chen, L. Ma, G. Ji, K. Chang and J. Y. Lee, *Mater. Today*, 2014, **17**(4), 184–193.
18 H. Li, K. Yu, H. Fu, B. Guo, X. Lei and Z. Zhu, *Phys. Chem. Chem. Phys.*, 2015, **17**(44), 29824–29833.
19 O. Eidelman, H. Friedman, R. Rosentsveig, A. Moshkovith, V. Perfiliev, S. R. Cohen and R. Tenne, *Nano*, 2011, **6**(04), 313–324.
20 M. Ratoi, V. B. Niste, J. Walker and J. Zekonyte, *Tribol. Lett.*, 2013, **52**(1), 81–91.
21 P. U. Aldana, B. Vacher, T. L. Mogne, M. Belin, B. Thiebaut and F. Dassenoy, *Tribol. Lett.*, 2014, **56**(2), 249–258.
22 L. Chang, H. Yang, W. Fu, N. Yang, J. Chen, M. Li and J. Li, *Mater. Res. Bull.*, 2006, **41**(7), 1242–1248.
23 O. Y. Posudievsky, O. A. Khazieieva, V. V. Cherepanov, G. I. Dovbeshko, A. G. Shkavro, V. G. Koshechko and V. D. Pokhodenko, *J. Mater. Chem. C*, 2013, **1**(39), 6411–6415.
24 D. Zheng, Z. Cai, M. Shen, Z. Li and M. Zhu, *Appl. Surf. Sci.*, 2016, **387**, 66–75.
25 G. S. Bang, K. W. Nam, J. Y. Kim, J. Shin, J. W. Choi and S. Y. Choi, *ACS Appl. Mater. Interfaces*, 2014, **6**(10), 7084–7089.
26 Y. Yan, X. Ge, Z. Liu, J. Y. Wang, J. M. Lee and X. Wang, *Nanoscale*, 2013, **5**(17), 7768–7771.
27 A. C. Ferrari, J. C. Meyer, V. Scardaci, C. Casiraghi, M. Lazzeri, F. Mauri and A. K. Geim, *Phys. Rev. Lett.*, 2006, **97**(18), 187401.
28 A. Eckmann, A. Felten, A. Mishchenko, L. Britnell, R. Krupke, K. S. Novoselov and C. Casiraghi, *Nano Lett.*, 2012, **12**(8), 3925–3930.
29 M. Guo, Z. Cai, Z. Zhang and M. Zhu, *RSC Adv.*, 2015, **5**, 101965–101974.
30 G. Li, C. Li, H. Tang, K. Cao, J. Chen, F. Wang and Y. Jin, *J. Alloys Compd.*, 2010, **501**(2), 275–281.
31 Y. Xu, X. Zheng, X. Hu, K. D. Dearn and H. Xu, *Wear*, 2014, **311**(1), 93–100.
32 C. Lee, Q. Li, W. Kalb, X. Z. Liu, H. Berger, R. W. Carpick and J. Hone, *Science*, 2010, **328**(5974), 76–80.
33 S. Kwon, J. H. Ko, K. J. Jeon, Y. H. Kim and J. Y. Park, *Nano Lett.*, 2012, **12**(12), 6043–6048.
34 D. Berman, A. Erdemir and A. V. Sumant, *Carbon*, 2013, **59**, 167–175.